EXPLORING SPIN DISORDER IN FERRIMAGNETIC IRON OXIDES USING STANDARD DFT AND ADVANCED COMPUTATIONAL METHODS

Valentína BERECOVÁ[1,2], Martin FRIÁK[1], Naděžda PIZÚROVÁ[1], Jana PAVLŮ[2]

[1]*Institute of Physics of Materials, v.v.i., Czech Academy of Sciences, Brno, Czech Republic, EU,* berecova@ipm.cz, friak@ipm.cz, pizurova@ipm.cz

[2]*Department of Chemistry, Faculty of Science, Masaryk University, Brno, Czech Republic, EU,* houserova@chemi.muni.cz

https://doi.org/10.37904/nanocon.2025.5181

Abstract

Spin disorder in ferrimagnetic iron oxides critically influences their electronic and magnetic properties, particularly at the nanoscale. In this work, γ-Fe_2O_3 was investigated using several density-functional approaches (PBE, PBE+U, PBE+D4, SCAN, SCAN-L, SCAN+rVV10, r²SCAN and HSE06) to identify methods capable of accurately reproducing its structural, magnetic, and electronic characteristics. The PBE functional provided the best structural agreement with experiment, while PBE+U and HSE06 most accurately described magnetic moments of –4.03/–4.06 μ_B (Fe^{tetra}) and 4.16/4.14 μ_B (Fe^{octa}). HSE06 yielded a band gap of 2.31 eV, in good agreement with the experimental value. Spin flip energetics revealed that spin realignment at tetrahedral sites is roughly twice (or more) energetically demanding than at octahedral sites; for example, under PBE+U, the energy cost is 667 meV for Fe^{tetra} and 364–414 meV for Fe^{octa}. Density of states showed that increasing spin disorder induces Fe 3*d*- and O 2*p*-derived in-gap states and can reduce the band gap up to 1.38 eV. To reduce computational cost, the CHGNet machine-learned potential was tested. While it fails to reproduce magnetic orientations, it substantially accelerates structural optimization. Overall, the results clarify the link between spin disorder and electronic structure in iron oxides and demonstrate how DFT and machine-learning methods can be combined to efficiently model complex magnetic behavior for future research.

Keywords: DFT, quantum mechanics, iron oxides, spin flip, magnetism, machine learning, neural network

1. INTRODUCTION

Iron oxide nanoparticles are a widely studied class of magnetic materials owing to their versatile applications in biomedicine [1,2] and energy storage [3], where magnetic and electronic properties are strongly influenced by particle size. Bulk maghemite (γ-Fe_2O_3) exhibits ferrimagnetic ordering, which arises from the antiparallel coupling between Fe^{3+} ions occupying tetrahedral (Fe^{tetra}) and octahedral (Fe^{octa}) sites within the inverse spinel lattice (**Figure 1a**). However, in ultrasmall iron oxide nanoparticles, the high surface-to-volume ratio leads to broken superexchange interactions through reduced atomic coordination and bond distortions, resulting in magnetically disordered layers and a measurable decrease in total magnetization [4]. Notably, such spin disorder has been associated with enhanced T_1 relaxation times in MRI, hinting at functional relevance [5].

Local spin flips - individual reversals of iron magnetic moments - represent the simplest microscopic manifestation of spin disorder, particularly within computational models constrained to collinear magnetism, where the magnetic moments cannot freely rotate in the *x* or *y* directions. Such disorder is metastable in the bulk but can become energetically stabilized in nanoparticles [6,7]. This stabilization is influenced by the nature of possible surface capping, which can modify the effect of dangling bonds on the electronic structure.

Since magnetism stems from the underlying electronic structure of material, alterations in spin alignment also manifest as changes in the density of electronic states (DOS), which can be further analyzed to assess the additional effect of spin disorder. To obtain an accurate description of the electronic states, band gaps and possible in-gap states, it is necessary to compare different density-functional approaches, as standard semi-local functionals tend to underestimate the band gap and misrepresent electronic properties in iron oxides [8]. The theoretical (quantum-mechanical) analysis was performed on bulk γ-Fe_2O_3, as the application of advanced methods is computationally demanding for larger spin-polarized models (nanoparticles).

2. COMPUTATIONAL METHODOLOGY

All quantum-mechanical calculations in this study were performed using Vienna *Ab initio* Simulation Package (VASP) [9,10] within the framework of density functional theory (DFT) [11,12]. The projector augmented wave (PAW) [13,14] pseudopotentials were applied with the 2*s* and 2*p* orbitals for oxygen and 3*d*, 4*s* and semicore 3*p* orbitals for iron treated as valence states. A plane-wave cutoff energy was 500 eV. Bulk γ-Fe_2O_3 structures were relaxed using the 6×6×6 Monkhorst-Pack k-point grid and tetrahedron method with Blöchl correction.

To evaluate the effect of the exchange-correlation contribution, several functional approximations were tested. The general gradient approximation (GGA) with Perdew-Burke-Ernzerhof (PBE) [15] parametrization served as the baseline. Dispersion corrections were included via the PBE+D4 scheme [16], which accounts for van der Waals pairwise interactions. The PBE+U approach of Dudarev *et al.* [17] was used to correct the self-interaction error and excessive delocalization of Fe 3*d* electrons through an on-site Coulomb term, employing U_{eff} = 4.3 eV. Beyond GGA, several meta-GGA functionals that incorporate the kinetic energy density were tested. These included strongly constrained and appropriately normed (SCAN) [18] functional, its deorbitalized version SCAN-L [19], the r^{2}SCAN [20] regularized form with higher numerical stability and SCAN+rVV10 [21] functional including nonlocal van der Waals correlation via the revised rVV10 kernel.

For higher-level calculations of the electronic structure, the HSE06 [22] screened hybrid functional was used, combining 25 % short-range Hartree-Fock exchange with PBE correlation. Static HSE06 calculations were carried out using the Γ-point-only setup due to the computational limitations with denser k-meshes. A Gaussian smearing scheme was used with a width of 0.05 eV to obtain the DOS with high accuracy.

Finally, a pretrained universal neural network potential for charge-informed atomistic modelling (CHGNet) [23] was used to compare the predicted structural and magnetic properties with DFT reference data, evaluating its ability to capture spin-related complexities.

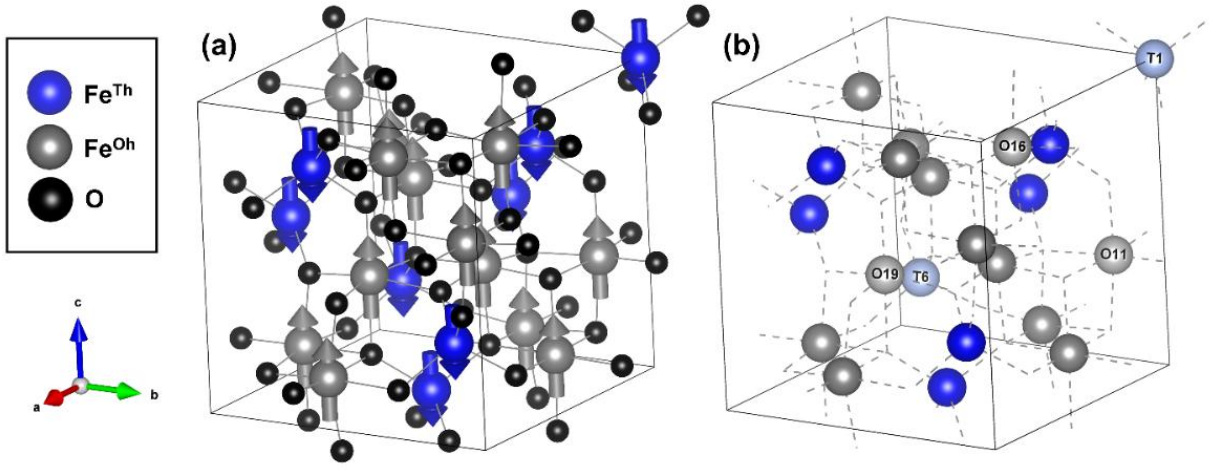

Figure 1 (a) Ferrimagnetic structure of bulk γ-Fe_2O_3 and **(b)** highlighted Fe atoms indicating the sites where individual spin flips were introduced, see the text below.

3. RESULTS

Before analyzing the influence of spin flips, it was necessary to identify a computational approach capable of reproducing structural and electronic properties consistent with experiment. The results obtained using various exchange-correlation functionals are summarized in **Table 1**. The PBE functional shows the best structural match, deviating only 0.18% in the lattice parameter. All functionals used for structural relaxation (except HSE06) predict a slight contraction of the unit cell, except for PBE+U, which yields expansion. The SCAN, SCAN-L and SCAN+rVV10 functionals lost the cubic symmetry, with the *c* parameter deviating from the ideal cubic arrangement by about 0.10-0.13 %. PBE+U and HSE06 best reproduce the magnetic moments, while other methods fail to capture their correct magnitudes. Nevertheless, their relative spin alignments were consistent, resulting in nearly identical total magnetizations across all approaches. PBE and PBE+D4 fail to reproduce the semiconducting character of maghemite, showing states at the Fermi level. Meta-GGA functionals and PBE+U perform moderately better in this aspect, whereas HSE06 gives a band gap of 2.31 eV closely matching the experimental optical value 2.2 eV. Since HSE06 functional is computationally demanding, only a static single-point calculation was performed on the PBE-relaxed structure, which already showed the best structural agreement with experiment.

Table 1 Calculated properties of bulk cubic γ-Fe_2O_3 obtained using different functionals. The table lists the optimized lattice parameter (*a*), its deviation from the experiment (a/a_{exp}), magnetic moments of Fe atoms at tetrahedral (Fe^{tetra}) and octahedral (Fe^{octa}) sites, magnetic moments of oxygen atoms and the total magnetic moment per conventional cell. The reported band gap values correspond to the indirect fundamental gap.

Functional	*a* (Å)	a/a_{exp} (%)	magnetic moment (μ_B)				band gap (eV)
			Fe^{tetra}	Fe^{octa}	O	cell	
PBE	8.3317	-0.18	-3.35	3.66	0.09	23.7	0
PBE+D4	8.2629	-1.01	-3.29	3.63	0.09	23.7	0
PBE+U	8.4392	1.10	-4.06	4.16	0.07	23.7	1.66
SCAN	8.2870	-0.72	-3.79	3.95	0.09	23.8	0.85
SCAN-L	8.2561	-1.09	-3.40	3.69	0.09	23.8	0.85
R^2SCAN	8.3028	-0.53	-3.79	3.95	0.09	23.8	0.87
SCAN+rVV10	8.2700	-0.92	-3.79	3.95	0.09	23.8	0.83
HSE06	-	-	-4.03	4.14	0.07	23.9	2.31

To further investigate the magnetic stability, the energetics of single spin flips were analyzed using PBE, PBE+U and r^2SCAN, which proved to be the most reliable functionals in the previous step. For each functional, five configurations with an individual spin flip were fully relaxed, with the flipped Fe sites indicated in **Figure 1b**. This approach allowed us to evaluate whether the energetic cost of a spin flip depends on its position within the lattice. **Table 2** shows that a spin flip in the tetrahedral sublattice is significantly more energetically demanding than in the octahedral sublattice across all tested methods. This trend corresponds well with experimental observations [24], where Mössbauer spectroscopy revealed that octahedral positions are more susceptible to spin canting than the tetrahedral ones. Furthermore, our calculations show that the spin flip energy varies among octahedral Fe sites, which arises from the structural non-equivalence caused by disordered octahedral vacancies (since cubic γ-Fe_2O_3 is derived from Fe_3O_4 by partial removal of Fe ions from the octahedral sites). Structural analysis of the spin-flipped models also revealed a deformation of the cubic lattice, likely caused by repulsive interactions introduced by the newly formed antiparallel spin pairs.

Table 2 Calculated energies per single spin flip (E_{flip}) for selected Fe sites in bulk γ-Fe_2O_3 using different exchange-correlation functionals. Each configuration contains one flipped spin in the entire unit cell, located either in the tetrahedral (T) or octahedral (O) sublattice.

Functional	E_{flip} (meV)				
	T1	T6	O11	O16	O19
PBE	1372	1372	260	260	325
PBE+U	667	667	364	364	415
R^2SCAN	949	949	523	523	591

Table 2 shows that the energies of individual spin flips vary across different functionals, while maintaining the same general trends: E_{flip} (T) > E_{flip} (O) and E_{flip} (O19) > E_{flip} (O11/O16). To further examine how collective spin flips influence the energy, configurations with simultaneous spin flips were generated and relaxed using the PBE and PBE+U functionals, while static HSE06 calculations were performed on the PBE-relaxed structures. Two models were constructed per functional: SP1, SP2 (PBE) and $SP1^U$, $SP2^U$ (PBE+U), each including spin flips in both the tetrahedral and octahedral sublattices in ratios 2:4 and 2:5, respectively. Configurations SP1 and $SP1^U$ involve only the change in orientation of the magnetic moment (e.g., from -4.1 μ_B to 4.1 μ_B), while SP2 and $SP2^U$ include a change in both orientation and magnitude (e.g., from 4.1 μ_B to -2.2 μ_B). This spin disorder results in a reduction of the total magnetization per unit cell by approximately 75-99% compared to the ferrimagnetic ground state. The corresponding energies per spin flip are 518 meV (SP1), 407 meV (SP2), 456 meV ($SP1^U$) and 490 meV ($SP2^U$). These results show that the energetic cost per flip is more consistent between functionals when multiple spins are reversed simultaneously. The energies of SP1 and SP2 configurations were previously presented in our earlier work [7] for comparison with nanoparticle models.

The electronic structure and band gap of the SP1 and SP2 configurations were analyzed by the density of states (DOS) (**Figure 2**) using HSE06, which proved to yield the most accurate bandgap. SP1 preserves a 2.55 eV band gap, which is slightly larger than in the ferrimagnetic bulk, with an in-gap state primarily originating from O orbitals and partially from the Fe^{octa} *d* orbitals. More differences appear in SP2, which exhibits the emergence of in-gap states that narrow the gap to 1.38 eV and increase the DOS asymmetry between the spin channels. In the case of SP2, these states mainly originate from Fe^{octa} *d* orbitals. The formation of in-gap states arises from the disruption of Fe 3*d*-O 2*p* hybridization caused by spin misalignment, while the additional change in Fe magnetic moment magnitude further shifts the 3*d* Fe states towards the Fermi level.

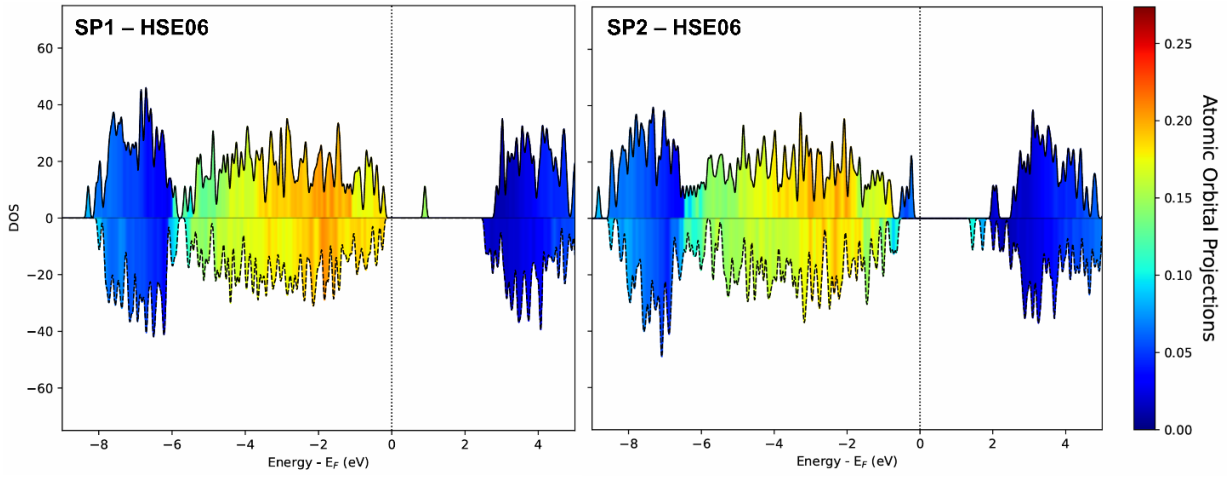

Figure 2 Spin polarized DOS of the SP1 and SP2 configurations calculated using the HSE06 functional on the PBE-relaxed structures. The colour scale represents the atomic orbital projections corresponding to oxygen atoms, highlighting their contribution to the valence and conduction bands.

We also tested a machine-learned interatomic potential on the $Fe_{45}O_{116}$ nanoparticle and its pseudo-hydrogenated form $Fe_{45}O_{16}psH_{96}$ from a previous study [7]. CHGNet was selected because it employs a charge-informed universal potential capable of predicting magnetic moments. However, our results revealed that it cannot capture magnetic moment orientations, making it unsuitable for systems with ferrimagnetic or spin-disordered character. Instead, we explored its applicability for pre-relaxation of spin-disordered structures, where it proved to be efficient for non-functionalized nanoparticles, achieving interatomic distances closer to the PBE results within a few seconds (**Figure 3a**). This pre-relaxation, followed by DFT refinement, could potentially reduce the overall computational time. The pseudohydrogenated model showed larger deviations (**Figure 3b**), likely because CHGNet does not account for the effective charge introduced by pseudohydrogen.

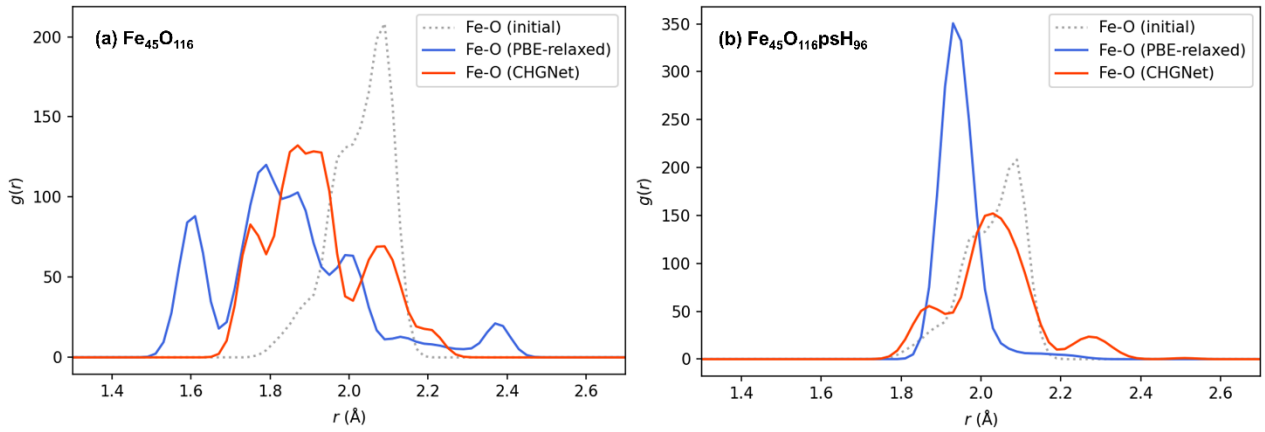

Figure 3 Radial distribution function (RDF) *g* for Fe-O in (a) $Fe_{45}O_{116}$ and (b) $Fe_{45}O_{116}psH_{96}$. The function *g* represents the probability density of finding a particle at the distance *r* from a reference particle.

4. CONCLUSION

This study systematically compared several density functional approaches to describe ferrimagnetic γ-Fe_2O_3. The PBE functional provided the best structural agreement, while PBE+U and HSE06 most accurately reproduced magnetic moments. The HSE06 functional also yielded a band gap of 2.31 eV, which is closest to the experimental value. Spin flip energetics revealed that tetrahedral Fe sites require roughly twice (or more) energy for spin realignment compared to octahedral sites. Multiple spin flips reduced the total magnetization by over 75 % and introduced in-gap states associated with disrupted Fe 3*d*-O 2*p* hybridization. The CHGNet model was evaluated as a fast pre-relaxation tool; however, due to its inability to capture spin orientation, it is not suitable for the accurate analysis of ferrimagnetic or spin-disordered systems.

ACKNOWLEDGEMENTS

N.P. and V.B. acknowledge the Czech Science Foundation for the financial support received under the project No. 21-31852J. M.F. acknowledges the financial support provided by the Czech Academy of Sciences (the Praemium Academiae). Computational resources were made available by the Ministry of Education, Youth and Sports of the Czech Republic under the Project e-INFRA CZ (ID:90254) at the IT4Innovations National Supercomputing Center, the MetaCentrum and CERIT-SC. Access to CESNET storage facilities provided by the project e-INFRA CZ under the program "Projects of Large Research, Development and Innovations Infrastructures" (LM2023054) is appreciated. The financial support provided by Masaryk University (project no. MUNI/A/1691/2024) is also acknowledged. The computational cells in Figure 1 were visualized by the VESTA package [25].

REFERENCES

[1] GUARDIA, P., DI CORATO, R., LARTIGUE, L., WILHELM, C., ESPINOSA, A., GARCIA-HERNANDEZ, M., GAZEAU, F., MANNA, L., PELLEGRINO, T. Water-soluble iron oxide nanocubes with high values of specific absorption rate for cancer cell hyperthermia treatment. *ACS Nano*. 2012, vol. 6, pp. 3080-3091.

[2] LAURENT, S., FORGE, D., PORT, M., ROCH, A., ROBIC, C., VANDER ELST, L., MULLER, R. N. Magnetic iron oxide nanoparticles: synthesis, stabilization, vectorization, physicochemical characterizations, and biomedical applications. *Chemical Reviews*. 2008, vol. 108, pp. 2064-2110.

[3] PRIYADARSHI, H., SINGH, K., SHRIVASTAVA, A. Experimental study of maghemite nanomaterials towards sustainable energy storage device application. *Materials Science in Semiconductor Processing*. 2022, vol. 147, pp. 106698.

[4] MORALES, M. P., VEINTEMILLAS-VERDAGUER, S., MONTERO, M. I., SERNA, C. J., ROIG, A., CASAS, L., MARTÍNEZ, B., SANDIUMENGE, F. Surface and internal spin canting in γ-Fe_2O_3 nanoparticles. *Chemistry of Materials*. 1999, vol. 11, pp. 3058-3064.

[5] WEI, H., WISNIOWSKA, A., FAN, J., HARVEY, P., LI, Y., WU, V., HANSEN, E. C., ZHANG, J., KAUL, M. G., FREY, A. M., ADAM, G., FRENKEL, A. I., BAWENDI, M. G., JASANOFF, A. Single-nanometer iron oxide nanoparticles as tissue-permeable MRI contrast agents. *Proceedings of the National Academy of Sciences of the United States of America*. 2021, vol. 118, pp. 2102340118.

[6] BIANCHETTI, E., DI VALENTIN, C. Effect of surface functionalization on the magnetization of Fe_3O_4 nanoparticles by hybrid density functional theory calculations. *The Journal of Physical Chemistry Letters.* 2022, vol. 13, pp. 9348-9354.

[7] BERECOVÁ, V., FRIÁK, M., PIZÚROVÁ, N., PAVLŮ, J., First-principles insights into structure and magnetism in ultra-small tetrahedral iron oxide nanoparticles. *Phys. Chem. Chem. Phys.* 2025, vol. 27, pp. 21424 – 21440.

[8] MENG, Y., LIU, X., HUO, C., GUO, W., CAO, D., PENG, Q., DEARDEN, A., GONZE, X., YANG, Y., WANG, J., JIAO, H., LI, Y., WEN, X. When density functional approximations meet iron oxides. *Journal of Chemical Theory and Computation*. 2016, vol. 12, pp. 5132-5144.

[9] KRESSE, G., HAFNER, J. Ab initio molecular dynamics for liquid metals. *Physical Review B*. 1996, vol. 47, pp. 558-561.

[10] KRESSE, G., FURTHMŰLLER, J. Efficient iterative schemes for ab initio total energy calculations using a plane wave basis set. *Physical Review B*. 1996, vol. 54, pp. 11169-11186.

[11] HOHENBERG, P., KOHN, W. Inhomogeneous electron gas. *Physical Review B*. 1964, vol. 136, pp. B864.

[12] KOHN, W., SHAM, L. J. Self-consistent equations including exchange and correlation effects. *Physical Review A*. 1965, vol. 140, pp. A1133.

[13] BLŐCHL, P. E. Projector augmented-wave method. *Physical Review B*. 1994, vol. 50, pp. 17953-17979.

[14] KRESSE, G., JOUBERT, D. From ultrasoft pseudopotentials to the projector augmented-wave method. *Physical Review B*. 1999, vol. 59, pp. 1758-1775.

[15] PERDEW, J. P., BURKE, K., ERNZERHOF, M. Generalized gradient approximation made simple. *Physical Review Letters*. 1996, vol. 77, pp. 3865-3868.

[16] CALDEWEYHER, E., MEWES, J., EHLERT, S., GRIMME, S. Extension and evaluation of the D4 London-dispersion model for periodic systems. *Physical Chemistry Chemical Physics*. 2020, vol. 22, pp. 8499-8512.

[17] DUDAREV, S. L., BOTTON, G. A., SAVRASOV, S. Y., HUMPHREYS, C. J., SUTTON, A. P. Electron-energy-loss spectra and the structural stability of nickel oxide. *Physical Review B*. 1998, vol. 57, pp. 1505-1509.

[18] SUN, J., RUZSINSZKY, A., PERDEW, J. P. Strongly constrained and appropriately normed semilocal density functional. *Physical Review Letters*. 2015, vol. 115, 036402.

[19] MEJIA-RODRIGUEZ, D., TRICKEY, S. B., Deorbitalized meta-GGA exchange-correlation functionals in solids. Physical Review B. 2018, vol. 98, pp. 115161.

[20] FURNESS, J. W., KAPLAN, A. D., NING, J., PERDEW, J. P., SUN, J. Accurate and numerically efficient r^2SCAN meta-generalized gradient approximation. *The Journal of Phys. Chem. Letters*. 2020, vol. 11, pp. 8208-8215.

[21] PENG, H., YANG, Z., PERDEW, J. P., SUN, J. Versatile van der Waals density functional based on a meta-generalized gradient approximation. *Physical Review X*. 2016, vol. 6, pp. 041005.

[22] KRUKAU, A. V., VYDROV, O. A., IZMAYLOV, A. F., SCUSERIA G. E. Influence of the exchange screening parameter on the performance of screened hybrid functionals. *The Journal of Chemical Physics*. 2006, vol. 125, pp. 224106.

[23] DENG, B., ZHONG, P., JUN, K., RIEBESELL, J., HAN, K., BARTEL, C. J., CEDER, G. CHGNet as a pretrained universal neural network potential for charge-informed atomistic modelling. *nature machine intelligence*. 2023, vol. 5, pp. 1031-1041.

[24] ROCA, A. G., NIZNANSKY, D., POLTIEROVA-VEJPRAVOVA, J., BITTOVA, B. GONZÁLES-FERNÁNDEZ M. A. Magnetite nanoparticles with no surface spin canting. Journal of Applied Physics. 2009, vol. 105, pp. 114309.

[25] MOMMA, K., IZUMI, F. VESTA 3 for three-dimensional visualization of crystal, volumetric and morphology data. *Journal of Applied Crystallography*. 2011, vol. 44, pp. 1272.